Highlights

An Accuracy Assessment of the Surface Reflectance Product from the EMIT Imaging Spectrometer

Red Willow Coleman, David R. Thompson, Philip G. Brodrick, Eyal Ben-Dor, Evan Cox, Carlos Pérez García-Pando, Todd Hoefen, Raymond Kokaly, John M. Meyer, Francisco Ochoa, Gregory S. Okin, Daniela Heller Pearlshtien, Gregg Swayze, Robert O. Green

- We present a performance assessment of the surface reflectance product from the EMIT imaging spectrometer onboard the International Space Station.
- EMIT surface reflectance at a typical arid land scene has a standard reflectance error of ±1.0% for coincident observations, rising to ±2.7% for data acquired on different dates and times of day.
- A comprehensive error budget encapsulates the differences between EMIT surface reflectance and in-situ field spectrometer measurements.

An Accuracy Assessment of the Surface Reflectance Product from the EMIT Imaging Spectrometer

Red Willow Coleman[a], David R. Thompson[a], Philip G. Brodrick[a], Eyal Ben-Dor[b], Evan Cox[c], Carlos Pérez García-Pando[d,e], Todd Hoefen[c], Raymond Kokaly[c], John M. Meyer[c], Francisco Ochoa[f], Gregory S. Okin[f], Daniela Heller Pearlshtien[b], Gregg Swayze[c], Robert O. Green[a]

[a]*Jet Propulsion Laboratory, California Institute of Technology, Pasadena, CA, USA*
[b]*Tel Aviv University, Tel Aviv, Israel*
[c]*U.S. Geological Survey, Denver, CO, USA*
[d]*Barcelona Supercomputing Center, Barcelona, Spain*
[e]*Catalan Institution for Research and Advanced Studies, Barcelona, Spain*
[f]*University of California Los Angeles, Los Angeles, CA, USA*

Abstract

The Earth surface Mineral dust source InvesTigation (EMIT) is an imaging spectrometer launched to the International Space Station in July 2022 to measure the mineral composition of Earth's dust-producing regions. We present a systematic accuracy assessment of the EMIT surface reflectance product in two parts. First, we characterize the surface reflectance product's overall performance using multiple independent vicarious calibration field experiments with hand-held and automated field spectrometers. We find that the EMIT surface reflectance product has a standard error of ±1.0% in absolute reflectance units for temporally coincident observations. Discrepancies rise to ±2.7 % for spectra acquired at different dates and times of day, which we attribute mainly to changes in solar geometry. Second, we develop an error budget that explains the differences between EMIT and in-situ field spectrometer data. We find that uncertainties in spatial footprints, field spectroscopy, and the EMIT-reported measurement were sufficient to explain discrepancies in most cases. Our approach did not detect any systematic calibration or reflectance errors in the timespan considered. Together, these findings demonstrate that a space-based imaging spectrometer can acquire high-quality spectra across a wide range of observational and atmospheric conditions.

Keywords: Imaging Spectroscopy, Remote Sensing, Surface Reflectance

1. Introduction

Visible-shortwave infared (VSWIR) Imaging Spectrometers are revolutionizing how we measure the Earth from space. These instruments can capture the full solar-reflected spectral range from 400-2500 nm, enabling measurements of diverse Earth surface processes. The associated science spans such varied fields as terrestrial ecology, aquatic biology, geology, and cryosphere science. They also address a host of societal applications related to natural hazards, agriculture, detection of greenhouse gas point sources, and more. This utility has led several space agencies to launch imaging spectrometers, including the Earth surface Mineral dust source InvesTigation (EMIT) [1], Environmental Mapping and Analysis Program (EnMAP) [2], Hyperspectral Imager Suite (HiSUI) [3], DLR Earth Sensing Imaging Spectrometer (DESIS) [4], and PRecursore IperSpettrale della Missione Applicativa (PRISMA). Future missions such as Copernicus Hyperspectral Imaging Mission for the Environment (CHIME) [5] and Surface Biology and Geology (SBG) [6] will provide global coverage at a regular cadence.

Historically, *atmospheric correction* has been one of the most challenging aspects of imaging spectrometer processing and data analysis. Imaging spectroscopy Earth surface studies generally operate on surface reflectance spectra which represent the fraction of incident illumination at the surface reflected back in the direction of the observer.

*Corresponding author: willow.coleman@jpl.nasa.gov

However, orbital sensors cannot measure this quantity directly - they measure only the illumination incident upon the sensor, which is influenced not just by surface reflectance but also by atmospheric absorption and scattering along the photon path from the sun to the ground to the sensor. This absorption and scattering changes rapidly in space and time, so imaging spectrometer studies of Earth's surface can use the spectrum itself to estimate and remove atmospheric interference. This process has been colloquially called atmospheric correction, though it is a model inversion problem by which the analyst uses spectroscopic data to estimate the surface reflectance and atmospheric state.

Atmospheric correction is critical in any imaging spectrometer study of Earth's surface. While there are several field campaigns to assess reflectance products from airborne imaging spectrometers, there are relatively few using the latest generation of orbital spectrometers. Alonso et al. [4] compare reflectance products from the DESIS visible-near infrared (VNIR) imaging spectrometer to data from two RadCalNet-managed calibration sites, finding differences in absolute reflectance that are generally less than 2%. Heller Pearlshtein and Ben-Dor [7] compare DESIS data with ground measurements in a more topographically complex scene, finding errors exceeding 5% for some wavelength regions but generally good spectral agreement and accuracy in resulting mineral products. Storch et al. [2] compare EnMAP imaging spectrometer data to ground reference spectra, and find one-sigma uncertainties between 1-4% depending on the surface cover and albedo. Cogliati et al. [8] characterize PRISMA's performance over ground validation sites, finding errors of 2-7% from in-situ data.

This paper builds on this growing body of work by validating orbital surface reflectance data from EMIT, an imaging spectrometer onboard the International Space Station [1]. EMIT was launched to the space station in July 2022 and delivered over 60,000 reflectance images for public use at the time of this writing. The EMIT program aims to measure the mineral composition of Earth's primary mineral dust source regions. This information, provided to Earth system models, will improve the prediction of mineral dust composition and consequent radiative forcing effects [9, 10]. Beyond these dust source areas, EMIT has measured regions spanning a wide range of surface types. Future expansions of the acquisition mask may provide even broader coverage.

EMIT has several characteristics that distinguish its surface reflectance products from previous orbital imaging spectrometers. It provides spectral wavelength calibration non-uniformity less than 2% of a channel width across the entire field of view, with a measured sampling of <7.5 nm and full-width half max (FWHM) of 8.5 nm [11]. Its Dyson optical layout provides high radiometric performance that provides ease of alignment and a low F-number (f/1.8), relative to earlier designs. Uniquely, it contains no shutter or onboard calibrators of any kind. Instead, the EMIT instrument design focuses on a simpler design with few components and thermal stability to enable vicarious calibration methods. It relies exclusively on vicarious calibration techniques for orbital dark frame characterization, flat field estimation, spectral calibration, relative radiometry, and absolute radiometry. On the data processing side, EMIT uses a probabilistic reflectance estimation approach based on Bayesian model inversion. Optimal estimation was pioneered decades ago for remote atmospheric sounding and adapted for VSWIR imaging spectroscopy in several airborne campaigns [12]. EMIT is the first orbital mission to use this approach operationally. Consequently, validation of EMIT reflectance spectra is an important pathfinder - of both the calibration concept and the atmospheric correction method.

This paper assesses the performance of EMIT surface reflectance products in two ways. First, we conduct multiple independent vicarious validation experiments that characterize EMIT reflectance performance for a representative range of scenes. We consider automated calibration network sites, manual measurement of traditional open playa validation sites, and several mixed vegetation wildland sites. We also assess the product repeatability and stability with measurements of pseudoinvariant Calibration Sites (PICS) where no ground truth data are available [13]. An analysis of temporally coincident EMIT observations in arid land regions at the core of the mission's science objectives demonstrates a reflectance product standard error of ±1.0%. This finding is broadly consistent with the first calibration studies conducted by the EMIT team [11]. This discrepancy grows to ±2.7% for observations at different dates and solar angles, which we attribute to real changes in the bi-directional reflectance distribution function (BRDF).

Our second contribution demonstrates an account of instrument and algorithm uncertainties that explain differences for these comparisons [14]. Analysis of PICS and playa acquisitions across multiple months indicates that most variance can be explained entirely by differing spatial footprints and forward-propagated measurement uncertainty, rather than systematic radiometric calibration error. A handful of outlier cases indicate challenging atmospheric conditions with phenomena outside the atmospheric model. These experiments demonstrate the power of a multi-site validation strategy for assessing satellite reflectance accuracy.

Section 2 describes the EMIT instrument and surface reflectance products. We then present our method for as-

sessing these reflectances, using both ground truth validation from multiple field campaigns and PICS [15]. We assess product accuracy and compare it to EMIT uncertainty predictions. We then close with an assessment of errors, both for the mineral products and other imaging spectroscopy user communities. We note several possible directions for future research to continue improving these reflectance products in the future (e.g., additional field campaigns and intercomparisons between EMIT and other orbital imaging spectrometers).

2. Methods

We develop a framework for systematically evaluating the current and long-term accuracy of EMIT's Level 2A (L2A) surface reflectance product by taking advantage of existing networks for vicarious calibration and strategically planned in-situ sampling efforts that align with EMIT acquisitions. To that end, we involve several sources of ground reference data. First, PICS are used to assess the effect of random errors on the EMIT surface reflectance product and to assess long-term drift in instrument calibration. Second, a set of field spectroscopy measurements of traditional desert playa sites and mixed-surface wildland sites are used to assess absolute radiometry. Finally, automated radiometric calibration sites (RadCalNet) provide ideal temporal coincidence for an accurate intercomparison that minimizes bi-directional reflectance distribution function (BRDF) discrepancies between the data sets. Each approach has a long history of use for remote satellite calibration.

In addition, we develop an error budget that explains the divergence in surface reflectance values between EMIT and the field sampled data. The evaluation between the EMIT surface reflectance product and Malvern Panalytical Analytical Spectral Devices FieldSpec, 4 Hi-Res NG Spectroradiometers with custom VNIR gratings (hereafter referred to as ASD spectrometers) or RadCalNet-measured surface reflectance, is a comparison between two measurement styles, rather than treating one as a ground truth product. We will demonstrate that the combined in-situ and EMIT error budgets are generally sufficient to explain the variability in surface reflectance between the two measurement types. The following sections describe our protocols for acquiring each of the remote and in-situ measurements, with attention to the possible error sources induced by each step.

2.1. EMIT Instrument

The EMIT instrument is a VSWIR imaging spectrometer. It measures the 380-2500 nm wavelength range at a sampling interval of approximately 7.5 nm. EMIT has a 75 km field of view on the Earth's surface, with approximately 60 meter ground sampling. It has a fixed nadir view on the International Space Station (ISS) and begins recording data whenever it passes over a section of the target mask. On-orbit experiments have demonstrated a spectral uniformity of better than 98% for channel wavelength center and FWHM [11]. Spectral response functions are Gaussian to within at least 0.1% of the peak magnitude [11]. Its Dyson optical design [16] provides high throughput (f/1.8) for optimal signal-to-noise ratios over dark surfaces. EMIT uses a multi-step radiometric calibration strategy where calibration coefficients are measured in the laboratory and then updated on orbit using vicarious methods [11]. At the time of this study, EMIT radiometric calibration has been updated only once at the start of the mission.

Despite EMIT's vicarious radiometric calibration approach, some systematic radiometric errors may remain in EMIT radiance data. First, the detector sensitivity may drift over time due to changes in the detector. Certain mercury-cadmium-telluride (HgCdTe) detectors can lose efficiency after exposure to high fluxes of blue and ultraviolet (UV) photons; this degradation in quantum efficiency (QE) is reversed only by thermally cycling the sensor from its operational cold state to ambient and back, a process which is performed very rarely by EMIT. While no blue QE degradation has been observed on EMIT, we aim to confirm this finding with a large validation data set. Second, the detector element gains themselves may drift. Electronic changes over day-to-month timescales can cause measurable changes in the relative response of different array elements [11]. EMIT compensates for this with a data-driven update of its flat field to preserve the uniformity of the array response. Third, vicarious calibration itself can be error-prone if atmospheric scattering over the calibration site is not modeled accurately. All of these errors would lead to systematic, spectrally-smooth deviations from the true radiometry, which would, in turn, affect surface reflectance spectra. Characterizing these errors requires validation with a larger population of scenes.

2.1.1. EMIT Surface Reflectance Product

The EMIT surface reflectance product processing pipeline uses the calibrated radiance at the sensor to infer the surface and atmospheric state. This procedure uses n measurement channels to infer n reflectance channels and additional atmospheric state parameters like the pressure elevation, column water vapor content, and aerosol optical depth. Because there are more unknowns than measurements, this mathematically under-determined problem requires additional constraints to solve. The EMIT reflectance product uses a Bayesian Maximum A Posteriori model inversion procedure, often called optimal estimation (OE) in the atmospheric remote sensing community [17]. Here, a prior distribution over surface reflectance provides a very weak constraint that reduces the effective number of degrees of freedom where the majority of channels are uncorrelated, except for several atmospheric windows in the near-infrared region with a block-diagonal covariance that enables the separation of surface reflectance and atmospheric signals. The EMIT algorithm uses a radiative transfer model based on sRTMnet [18], a machine learning-based emulator of the MODTRAN radiative transfer model [19]. The model inversion process optimizes the posterior probability of the state vector given the measurement. To date, the OE approach used by EMIT has been validated in airborne campaigns for terrestrial environments [12, 20, 21] and aquatic scenarios [22, 23, 24].

The EMIT data volumes require additional consideration. EMIT leverages the fact that the atmosphere changes over larger spatial scales more so than the instrument spatial sampling [21]. Consequently, it is only necessary to calculate the complete surface and atmosphere solution at a subset of spatial locations. EMIT fragments the image into spatial pixel clusters known as superpixels, each solved independently and containing roughly 40 EMIT pixels. Then, it interpolates the resulting atmospheric field to all native pixels and solves the surface reflectance portion of their state vector with a simple closed-form expression. In addition to accelerating the pixel-wise solution, this two-step strategy approximates the complete solution that would be obtained if all pixels in the image were solved simultaneously while respecting atmospheric smoothness constraints between neighbors [25]. We refer the interested reader to Brodrick et al. [26] for a complete description of the EMIT surface reflectance product.

The EMIT products report channel-wise uncertainties for each reflectance spectrum. This uncertainty is the diagonal of the full posterior uncertainty covariance matrix, $\hat{\mathbf{S}}$:

$$\hat{\mathbf{S}} = (\mathbf{K}^T \mathbf{S}_\epsilon \mathbf{K} + \mathbf{S_a}^{-1})^{-1} \tag{1}$$

where $\mathbf{K}$ is the Jacobian representing the partial derivative of radiance for each state vector element; $\mathbf{S}_\epsilon$ is the instrument radiance measurement uncertainty, and $\mathbf{S_a}$ is the prior covariance matrix. The instrument measurement uncertainty further decomposes into three terms:

$$\mathbf{S}_\epsilon = \mathbf{S_e} + \mathbf{S_{osf}} + \mathbf{S_d} \tag{2}$$

where $\mathbf{S_e}$ is instrument noise, derived from the model validated in Thompson et al [11]; $\mathbf{S_{osf}}$ is uncertainty induced by the boundary of an order sorting filter in the spectrometer, which is zero in everywhere except a few channels near 1290 nm, where it is high; and $\mathbf{S_d}$ is a model difference term meant to capture the offset between the modeled physics simulation and the true physics of the atmosphere. In addition to the instrument noise and model difference errors, there are other potential sources of atmospheric correction uncertainty not captured in the product posterior covariance matrices. First, EMIT's atmospheric model does not represent the wide range of aerosol optical properties on Earth's surface. It uses a simple scattering aerosol derived from sulfate optical properties [21], which performs well across a wide range of environments. Second, there are other radiative transfer approximations not captured in the $\mathbf{S_d}$, such as the resampling of optical coefficients to instrument wavelengths (rather than conducting all calculations at the highest possible spectral resolution). Alternatively, MODTRAN scalar code could be used rather than a polarization-sensitive vector code to calculate Rayleigh scattering. Unlike radiometric errors, which are systematic over timescales of days to weeks, these atmospheric correction errors will likely manifest differently with each acquisition due to changing atmospheric conditions. Thus, one can use the time dimension to assess the relative contribution of these uncertainties based on a combination of pseudoinvariant and ground-truthed playa sites.

The total error budget for comparisons with ground measurements must include these instrument errors reported in EMIT products and discrepancies expected from the differing fields of view. The error budget was calculated separately for EMIT and ASD reflectance measurements. Non-systematic error sources for each instrument are assumed to be independent, allowing for combination in quadrature to estimate total instrument error. The total EMIT surface reflectance error budget for intercomparisons, $\sigma_{\mathbf{EMIT}}$ is given by:

$$\sigma_{\mathbf{EMIT}} = \sqrt{\mathbf{S}_\epsilon + \sigma^2_{\mathbf{surf}}} \tag{3}$$

where $\mathbf{S}_\epsilon$ is the channel-wise forward-propagated instrument and measurement uncertainty. The $\sigma_{\mathbf{surf}}$ term is a post-hoc channel-wise estimation of local surface inhomogeneity that varies from 0-2.5%. It intends to capture the errors induced by any misalignment between the remote selected region, composed of discrete pixels, and the ground data. We calculated $\sigma_{\mathbf{surf}}$ with a bootstrapping approach to estimate the variance in the mean spectrum induced by surface reflectance variability at the site [27]. For a region consisting of n pixels, we randomly resampled the data with replacement and calculated the standard deviation of the resulting averaged surface reflectance pixels.

2.2. Pseudoinvariant Calibration Sites (PICS)

PICS have been extensively used for in-flight radiometric calibration of optical satellite sensors [13]. PICS are spatially uniform, spectrally stable, and relatively invariant with time. These sites may be used for multi-sensor cross-calibration, absolute radiometric calibration, and long-term trend analysis [15]. Recent research has confirmed that the twenty high-reflectance desert sites are still relevant targets for on-orbit calibration, nearly 30 years later [28]. Out of the original twenty PICS in the Sahara Desert and the Arabian Peninsula, six have been endorsed by the Committee on Earth Observation Satellites (CEOS) as the highest-quality standard reference sites for post-launch vicarious calibration [29].

Site name	Coordinates	# of acquisitions
Algeria-3	30.32°, 7.66°	11
Algeria-5	31.47°, 1.78°	12
Libya-1	24.42°, 13.35°	6
Libya-4	28.55°, 23.39°	13
Mauritania-1	19.4°, -9.3°	7
Mauritania-2	20.85°, -8.78°	5

Table 1: CEOS-endorsed pseudoinvariant calibration sites used for post-launch vicarious calibration and the number of cloud-free EMIT acquisitions within the first 300 days on orbit.

PICS were originally designated for assessing the radiometric calibration of lower-resolution Earth-observing satellites (e.g., AVHRR, Meteosat, MERIS) and span large desert areas of roughly 100 km x 100 km. As such, while PICS may be close enough to spatially uniform for satellites with a 1-2 km resolution, shifts in desert geomorphology over time will be more obvious at EMIT's 60 m pixel resolution. Most of the PICS contain large dunes and other sand features that are prone to changing and can induce directional effects that can obscure meaningful trends in radiometric calibration. Cosnefroy et al. points out that finer spatial resolution imagery should be averaged over a sufficiently large geographic area to minimize spatiotemporal variability due to geomorphology [13].

Following Cosnefroy et al.'s [13] guidance that finer spatial resolution imagery (e.g., EMIT's 60 m pixels) should be spatially averaged to reduce variability due to geomorphology, an average surface reflectance product of all EMIT overpasses for a given pseudoinvariant site will act as the "ground truth" product. Assuming that the pseudoinvariant sites are truly homogeneous, comparing the average surface reflectance from a given EMIT acquisition to the average surface reflectance of all EMIT acquisitions overlapping that site provides an estimate of error due to random atmospheric correction and instrument noise errors. In addition, the precessing orbit of the ISS enables repeat acquisitions over North Africa to assess whether EMIT's surface reflectance product at selected pseudoinvariant sites is stable over its first 300 days in orbit. Only scenes that were at least 90% cloud-free were used. Each pseudoinvariant site had at least six spatially coincident EMIT acquisitions, including some sites that were imaged twice on the same day. The area of interest was defined according to the CEOS region of interest recorded on the U.S. Geological Survey (USGS) cal/val site (https://www.usgs.gov/calval).

2.3. RadCalNet

The Radiometric Calibration Network (RadCalNet) is a set of four global sites that collect automated surface and atmosphere in-situ data to support vicarious optical calibration in the VSWIR range [30]. Each RadCalNet site provides bottom-of-atmosphere (BOA) reflectance spectra and relevant uncertainties at 10 nm sampling intervals from

the region of 400 nm to 1000 nm (up to 2500 nm at some sites) every 30 minutes, as well as aerosol optical properties and basic meteorological data. Due to quality control efforts, the true gap between subsequent surface reflectance measurement times is often much longer. However, this still provides the best spatiotemporal coincidence of any ground truth experiment. Here, we favor the Railroad Valley RadCalNet site in Nevada, USA. Railroad Valley Playa (RVUS) is located at (38.497°, -115.69°) and is operated by the University of Arizona. RVUS's BOA reflectance measurements are representative of the 1 square km site in central Nevada, USA. from 400 nm to 2300 nm. RadCalNet BOA simulated spectra are representative of nadir observations, which is broadly consistent with EMIT's nadir view and 75 km field of view. The provided RVUS International System of Units (SI)-traceable BOA uncertainty product provides an associated error budget. The other RadCalNet sites (La Crau, France, Gobabeb, Namibia, and Baotou, China) were not considered due to the spectral range of the RadCalNet radiometers and scene homogeneity considerations.

For the RadCalNet overpass, we selected EMIT pixels assuming that the ground reference data represented a 1-kilometer square area centered on the target. The ideal EMIT scenes for comparison against the calibration data sets were spatiotemporally coincident and cloud-free. In the case that these scenes were not available, spatially coincident and at least 50% cloud-free scenes were used. An acquisition from August 3, 2022 appeared in another independent study [11], so we ignore it here. We used nearest-neighbor resampling within the 1 km target area to compare EMIT data acquired at 7.5 nm sampling intervals with the RadCalNet data and associated BOA uncertainty at 10 nm sampling intervals.

2.4. ASD Field Spectroscopy

In addition to analyzing the automated and PICS sites, the EMIT science team conducted experiments using ASD spectrometers for in-situ surface reflectance measurements. We began with desert playa sites; these are commonly used for vicarious calibration of on-orbit reflectance products due to their inherent homogeneity [Figure 1]. In addition, playas are typical of arid mineral dust-forming areas for which high-quality and accurate surface reflectance data are critical to meet EMIT's science goals. Five in-situ desert playa sites were sampled in August 2022 in Israel and the southwestern United States [31, 32, 33, 34], within a month of EMIT's first-light imagery. An additional playa site in California was sampled in April 2023 [35]. At each site, the field team used a leveled spectralon panel as a white reference reflectance standard. They walked in a coverage pattern around an area of approximately 4 x 4 EMIT pixels, acquiring regular reference measurements of the spectralon target. The average reflectance of the 240 m by 240 m area was calculated during post-processing. See [35] for a detailed description of the methods used during the collection and processing of field site spectral measurements.

Figure 1: In-situ sampling field photo of Smith Creek, USA. Smith Creek Playa is a dry lake bed in central Nevada that is approximately 18 square miles. Photo credit: R. Kokaly.

An additional set of transect samples were acquired in March and April 2023 across various land cover conditions in the southwestern USA. The selected sites were all large and spatially flat. Unlike the spatially homogeneous playa

sites, these sites were located in wilderness landscapes with a mixture of sparse vegetation and soil. Consequently, the field team used a slightly different sampling strategy to account for the heterogeneity of the surface. The field team carried a spectrometer along a series of three 60 m transects set at 120-degree angles from each other, radiating out from a central point of known latitude and longitude. The team walked each transect acquiring periodic spectra in a line that crossed both plants and bare soil. The resulting spectra were converted to reflectance using periodic acquisitions of the reference panels and averaged into a mean spectrum for the area.

The ASD surface reflectance error budget, $\sigma_{\mathbf{ASD}}$ is given by:

$$\sigma_{\mathbf{ASD}} = \sqrt{\sigma_{\mathbf{spc}}^2 + \sigma_{\mathbf{rfl}}^2} \tag{4}$$

where $\sigma_{\mathbf{spc}}$ is a 1% error in spectralon reference BRDF [12, 36], and $\sigma_{\mathbf{rfl}}$ is a 2% ASD absolute reflectance uncertainty capturing instrument instabilities, any nonlinearities, and variability in the manual measurement protocol [37].

For each of the ASD field measurements, a corresponding study bounding box was recorded by GPS and used to compare against EMIT surface reflectance products. Only EMIT pixels with a sufficient number of ASD measurements ($n > 20$) were included in the sample to minimize edge effects. ASD data were resampled to EMIT wavelengths by nearest neighbor spectral resampling.

3. Results

3.1. Radiometric Stability

Figure 2 shows the reflectance values at each of the six pseudoinvariant sites across the desert regions of North Africa, plotted as a ratio of the average spectrum for each site. Acquisitions tend to group in time due to the precessing ISS orbit and seasonal drift in solar angles. Generally, the surface reflectance product is stable over time, and results are repeatable at multiple sites. Acquisitions within close temporal proximity are generally similar within +/- 2% in relative terms, or closer to 1% in absolute units. The EMIT acquisitions that show substantial deviations from the mean (e.g., Libya-1 and Algeria-5) had reflectance spectra that were vertically shifted in magnitude but maintained the same spectral shape, suggesting that variability in sun position or zenith angle may be an important contributing factor. Applying the solar zenith angle derived $\mathbf{S_{BRDF}}$ uncertainty term reveals that typical BRDF errors of $3-5\%$ are sufficient to explain much of the variability between temporally disparate EMIT acquisitions at these pseudoinvariant sites.

3.2. Vicarious Calibration at Desert Playa Sites

A visual and statistical intercomparison of EMIT and field spectrometer surface reflectance values shows good alignment. Wavelengths of known large atmospheric absorption (e.g., water vapor) were ignored (1320-1440 nm and 1770-1965 nm). EMIT surface reflectance values average 2.7% mean absolute error (MAE) for the selected in-situ playa sampling locations [Table 2]. Long Valley, Nevada showed the best agreement between ASD and EMIT surface reflectance values ($MAE = 0.87\%$). Smith Creek, Nevada had the least agreement between ASD and EMIT ($MAE = 4.41\%$). These discrepancies exceed EMIT's forward-propagated measurement error, but become consistent after sources of experimental uncertainty are included. Moreover, the absolute error includes BRDF changes due to differences in solar positions across EMIT and ground acquisitions, which would introduce some discrepancies even if the measurements were perfect.

A closer look at the spectral signatures of the six desert playa sites reveals that the shape of the reflectance spectrum closely matches between the in-situ and EMIT measurements. The EMIT spectra have several magnitude differences relative to the in-situ data, particularly in the SWIR region [Figure 3]. This region is traditionally challenging to accurately retrieve reflectance measurements due to atmospheric absorption and lack of photons towards the upper end of EMIT's spectral range. Despite the discrepancies, the 2σ error budget fully encapsulates the differences between field spectrometer and EMIT surface reflectance values, except for a few data points at the ends of EMIT's spectral range or near known atmospheric absorption features. A more comprehensive assessment of the absolute differences between the ASD and EMIT-measured reflectance spectra is apparent in [Figure 4]. While the absolute difference in surface reflectance measurements between EMIT and ASD at the desert playa sites ranges from roughly -10 to 5%, the spectral derivative of the absolute difference is closer to $\pm 1\%$, with some slightly higher errors towards the upper end

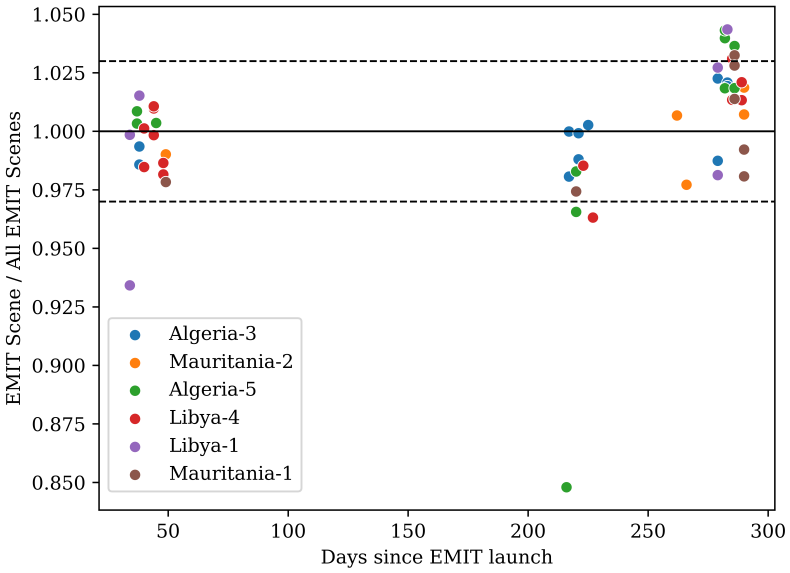

Figure 2: Relative difference between of scene-averaged surface reflectance and the average surface reflectance of all EMIT acquisitions at that location for PICS Algeria-3, Algeria-5, Libya-1, Libya-4, Mauritania-1, and Mauritania-2. Dashed lines show 3% agreement between EMIT surface reflectance values over time.

Site name	EMIT Date	ASD Date	MAE	EMIT SZA	Coordinates
Amiaz Plain	2022/08/14	+8 days	2.77%	52.97°	(31.068°, 35.372°)
Carson Sink, NV	2022/08/14	+3 days	1.17%	43.04°	(40.037°, −118.255°)
Coyote Lake, CA	2023/04/15	+2 days	2.22%	43.87°	(35.065°, −116.742°)
Edwards Creek, NV	2022/08/14	+5 days	4.25%	43.41°	(39.607°, −117.700°)
Long Valley, NV	2022/08/22	+1 day	0.87%	31.73°	(41.690°, −119.801°)
Smith Creek Valley, NV	2022/08/14	+4 days	4.41%	55.97°	(41.690°, −119.801°)

Table 2: Desert playa vicarious calibration sites in Israel and the USA show MAE values less than 4.5% for intercomparison of EMIT and ASD surface reflectance values. The elapsed time between in-situ sampling and the closest cloud-free EMIT scene is, at most, eight days. The solar zenith angle (SZA) of selected EMIT acquisitions varies from 31.73° to 55.97°.

of the SWIR range. Magnitude shifts in surface reflectance measurements are often corrected via continuum-removal or normalization methods. The spectral derivative of the absolute difference between ASD and EMIT reflectance gives an important metric of the high-frequency (wavelength-to-wavelength) noise that is often more detrimental to downstream analyses.

$$\textbf{Spectral Derivative} = \frac{\boldsymbol{\Delta}\textbf{(EMIT} - \textbf{ASD)}}{\boldsymbol{\Delta}\textbf{Channel}} \tag{5}$$

The RVUS automated site provides BOA reflectance spectra representative of a nadir view observation every 30 minutes. This provides near-perfect temporal coincidence, mitigating the effects of solar angle changes. A spatially and temporally coincident RVUS BOA measurement and EMIT overpass on June 12th, 2023 at 16:00 UTC shows good agreement between the two surface reflectance measurements [Figure 5]. The relative ratio between EMIT and RVUS surface reflectance measurements averaged across all bands except those of known atmospheric absorption is 0.981 ± 0.04 at the 1σ level. The corresponding absolute ratio between EMIT and RVUS is -0.006 ± 0.13 at the 1σ level. The surface reflectance products diverge slightly in the SWIR region, where EMIT reports lower surface reflectance values than RadCalNet.

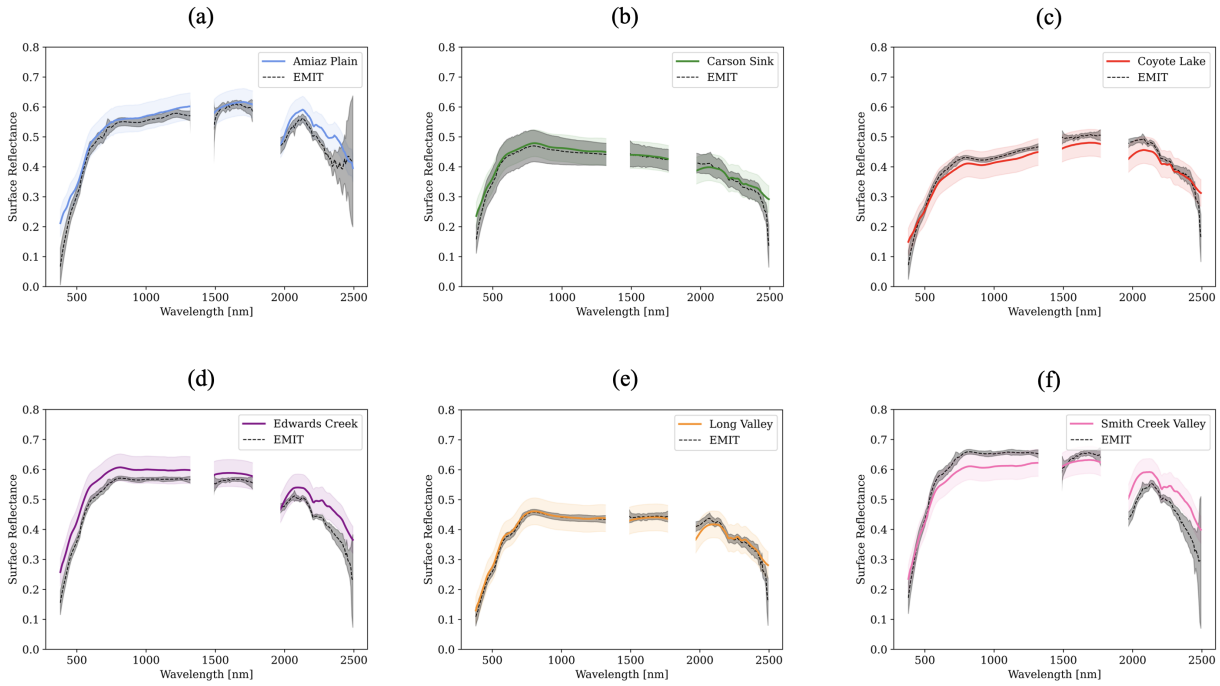

Figure 3: Direct comparison of in-situ ASD surface reflectance (solid color lines) and EMIT surface reflectance (dashed black lines) products at six desert playa sites. The shaded regions demarcate a 2σ uncertainty. (a) Amiaz Plain, Israel, (b) Carson Sink, Nevada, (c) Coyote Lake, California, (d) Edwards Creek, Nevada, (e) Long Valley, Nevada, (f) Smith Creek Valley, Nevada.

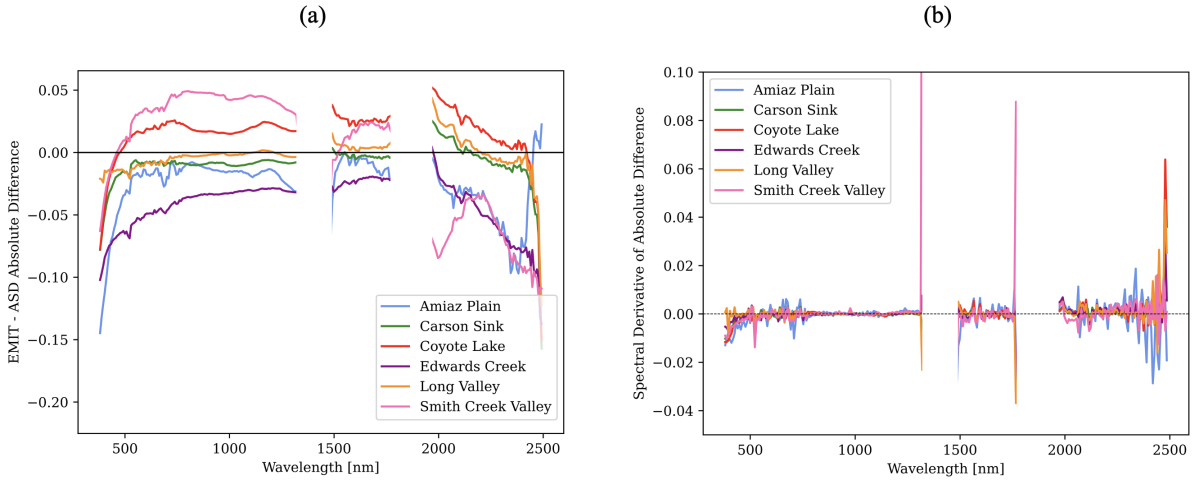

Figure 4: (a) Absolute difference between EMIT and ASD surface reflectance measurements at six desert playa sites in the US and Israel. (b) Spectral derivative of the absolute difference between EMIT and ASD measurements at the same playa sites.

Although the shape of spatially co-located EMIT and in-situ measurements are quite similar, magnitude shifts between the two surface reflectance spectra within the range of ±10% were observed at the desert playa sites. This is consistent with changes expected due to varying solar zenith angles from data acquired at different times of day. It is similar to the magnitude variability of BOA surface reflectance measurements at the RVUS RadCalNet site between 9:00 and 15:00 local time on a given day, where similar magnitude shifts across the spectral range are common. The

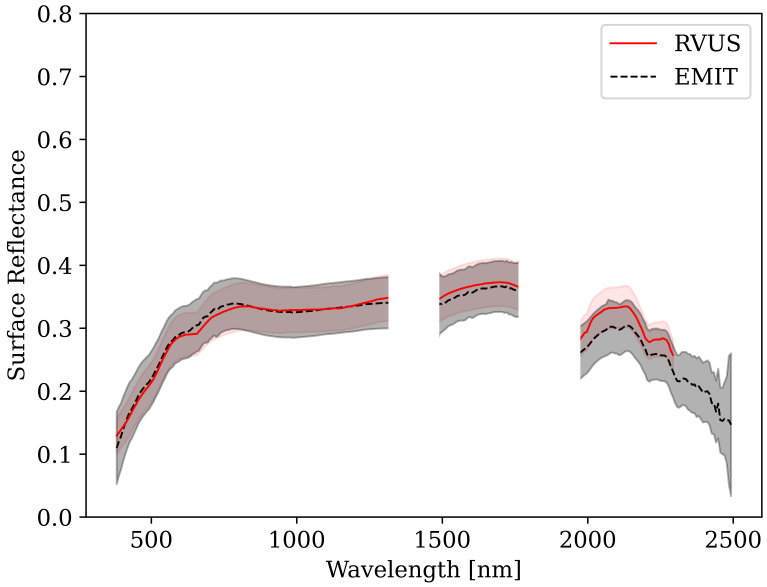

Figure 5: Comparison of RadCalNet bottom-of-atmosphere (BOA) reflectance at Railroad Valley Playa (RVUS, red line) to the surface reflectance of a spatiotemporally coincident EMIT overpass (black line) on 2023/06/12 at 16:00 UTC. The shaded regions (i.e., both gray and red) demarcate a 2σ uncertainty.

absolute reflectance values at RadCalNet sites can vary by up to 50% at certain wavelengths and times of day, but variability is usually $< 5\%$ within a given 30-minute period [30]. This is consistent with our assessment that RVUS data acquired $>$ 1 hour apart from a co-located EMIT overpass diverged substantially. Variability in RadCalNet magnitude at RVUS within a given day is typically largest in the SWIR, the spectral region where spatiotemporally co-located EMIT and RadCalNet surface reflectance measurements diverged the most. Likely, BRDF effects or pixel shadowing between an EMIT acquisition and co-located field measurements induce these magnitude shifts. Vegetation may induce additional shading and changes in vegetation phenology over time at mixed vegetated vicarious calibration sites.

3.3. Vicarious Calibration at Natural Arid Land Sites

In contrast to traditional desert playa vicarious calibration sites that are highly homogeneous, a comparison to field spectrometry data from mixed vegetation and soil across the southwestern United States. validates EMIT's surface reflectance data in natural arid landscapes. The MAE for a heterogeneous desert vegetation site near Little Lake, California was 0.9% for near-coincident EMIT and ASD measurements on April 15th, 2023 [Figure 6]. Similar to the desert playa sites, the 2σ error budget fully encapsulates the differences between the field spectrometer and EMIT surface reflectance values at a mixed vegetation site. In addition, when looking at EMIT's subsequent acquisitions at the same location, the spectral shape between subsequent EMIT acquisitions is consistent over time, though there are magnitude shifts, which could be explained by changes in BRDF or solar zenith angle. Additionally, vegetation in California's arid areas often experiences rapid growth and senescence that can be observed with imaging spectrometers [38].

4. Discussion

Intercomparison of EMIT surface reflectance data, handheld ASD spectrometers, and reflectance data from vicarious calibration sites showed good spectral alignment, particularly when the data were acquired simultaneously. When data were not acquired simultaneously, these measurements were still consistent with EMIT uncertainty products

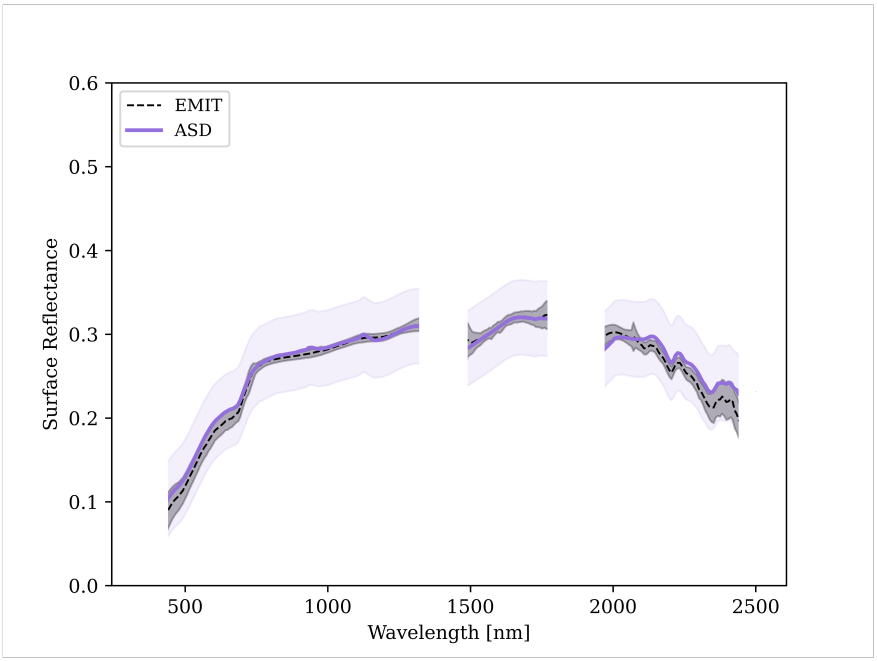

Figure 6: Direct comparison of in-situ ASD surface reflectance (solid color line) and EMIT surface reflectance (dashed black line) product near Little Lake, California. Both EMIT and ASD measurements were acquired on 2023/04/15. The shaded regions demarcate a 2σ uncertainty.

once instrument uncertainties were included. We could not detect any systematic bias of surface reflectance values across EMIT's measured spectral range. The optimal estimation approach for surface reflectance retrieval has been previously validated for an airborne imaging spectrometer in various challenging atmospheres [39]. EMIT surface reflectance matches well with in-situ data in various land cover types and aerosol conditions. For instance, the Amiaz Plain vicarious calibration site in Israel is an area of higher mean aerosol optical depth (AOD) than playa sites in the United States. and has a comparable MAE value for EMIT and in-situ surface reflectance measurements [40]. While it is possible that atmospheric conditions could affect the absolute accuracy of the surface reflectance product in areas of very high aerosol loading (e.g., Southeast Asia), accurate retrievals of surface reflectance affected by a wildfire smoke plume have been performed using an optimal estimation approach [41]. In such conditions, not represented in our data set, instrument and measurement noise are likely a very small portion of the total error budget in the EMIT surface reflectance product. The EMIT surface reflectance product algorithm is still in development, and for a more in-depth discussion of planned algorithm improvements, we refer the interested reader to Brodrick et al. [26].

4.1. Analysis of Error Sources

There are inherent assumptions in the optimal estimation atmospheric correction approach that may cause spectral shifts under certain observing conditions. The implemented optimal estimation approach assumes that the surface is Lambertian, and is not always valid at higher atmospheric loading conditions and large solar zenith angles [12]. It can also be challenging to simultaneously retrieve atmospheric and surface reflectance properties at sites located below sea level due to model assumptions (e.g., Amiaz Plain is roughly 250 m below sea level). In addition, the machine learning-based emulator of the MODTRAN radiative transfer model used for EMIT's surface reflectance retrieval assumes a single sulfate-like scattering aerosol [18]. In reality, the characteristics and quantity of atmospheric aerosols are more diverse, including directly emitted natural aerosols (e.g., dust and sea salt) and those formed by chemical reactions (e.g., nitrates and ammonium) [42]. Black carbon is an example of a light-absorbing aerosol, unlike a light-scattering aerosol like sulfate. Given EMIT's primary focus on Earth's dust-forming regions, future work could clarify the effect of different atmospheric aerosols, like coarse dust, on surface reflectance retrievals.

In addition, most 60 m x 60 m EMIT surface reflectance pixels are mixed, meaning there are multiple mineralogical or land cover features within a single pixel. While desert playa sites are largely homogeneous, collecting in-situ field

spectrometer data that align with a single EMIT pixel is challenging. This is why a larger region of 4 pixels by 4 pixels was sampled at desert playa sites in the southwestern United States. We attempted to limit the effect of mixed playa and non-playa pixels in our analysis by only including EMIT pixels with a sufficient number of in-situ measurements. For example, a visual assessment of the in-situ measurement area and a quantitative bootstrapping-based analysis confirmed that Carson Valley had higher surface inhomogeneity than other playa regions when all EMIT pixels within the sampling region were included, regardless of the number of in-situ samples. This suggests that EMIT is sensitive to spatial footprint alignment when the study area is relatively small and mixed vegetation and playa pixels exist. Future work could examine the influence of mixed vegetation and soil pixels on EMIT's higher-level mineralogy products will be the focus of a future study.

4.2. Spectral Magnitude Shifts in Imaging Spectroscopy Data

Magnitude discrepancies in spectral surface reflectance could have a range of causes, including calibration error and atmospheric aerosol uncertainty. In our experiments, the most prominent cause is probably a true change in the BRDF due to differences in solar angle between the remote and in-situ measurements. Unlike sun-synchronous satellites, the EMIT instrument observes the surface at many different local times which can lead to a wide range of solar-incidence angles. Consequently, accounting for BRDF is important for comparing EMIT measurements to each other (for pseudoinvariant sites) or measurements made in situ at different times of the day. An assessment of historical RVUS spectra from different solar angles indicated that ten degrees of solar zenith difference led to a 1% difference in the measured reflectance. The true relationship could differ depending on surface roughness, soil composition, and other playa properties. However, this simple heuristic is enough to explain observed errors. Reassuringly, the magnitude shift is effectively removed for the RVUS observation that is perfectly simultaneous.

Even sun-synchronous missions cannot escape variability in solar-observer geometry across latitudes, so algorithmic measures are needed to deal with the intrinsic variability in the hemispherical-directional reflectance factor (HDRF) that measures an aspect of the BRDF. The effect of observed spectral magnitude shifts between non-temporally coincident EMIT and in-situ field spectrometer measurements can be reduced by spectral normalization techniques. The primary use of the EMIT surface reflectance product is to measure the mineral composition of Earth's primary dust source regions to better constrain dust radiative forcing in Earth system models. The USGS Tetracorder system for mineral identification that EMIT uses relies on continuum-removed spectra that are relatively invariant to magnitude shifts [43]. This holds because the shape of the spectra is typically more important for mineral characterization than spectral brightness, particularly for minerals in the SWIR region [44]. Continuum removal minimizes the effects of BRDF and sun angle, allowing for more accurate identification of unique mineralogical spectral features [43].

Continuum removal normalization is important for mitigating the effects of spectral magnitude shifts in research fields beyond mineralogy, including cryosphere and terrestrial ecology [45]. Building and vegetation shade can cause magnitude shifts between spectra of the same land cover type, underscoring the need for spectral normalization [46]. For example, applying continuum removal to spectra before multiple endmember spectral mixing analysis (MESMA) for characterizing vegetation types from imaging spectroscopy can improve class separability in scenes with heterogeneous land cover [47]. Spectral magnitude shifts due to variable scene brightness are common for airborne imaging spectrometers, and it is not surprising that they are also observed in EMIT surface reflectance data.

We see the largest divergence between ASD and EMIT surface reflectance measurements in the SWIR region of the spectra. First, the SWIR has challenging retrieval conditions for optimal estimation caused by fewer photons and atmospheric absorption features towards the upper end of EMIT's spectral range [39]. Similarly, the ASD measurements in the SWIR region often have a lower signal-to-noise ratio (SNR) than other portions of the VSWIR spectra due to the same challenging atmospheric effects [48].

Lastly, the ISS's unique orbit means that repeat overflights of the same location rarely occur at the same time of day. While repeat acquisitions are rarely captured within the same day, they have occurred in the EMIT data archive. A closer look at inter-acquisition magnitude variability concerning acquisition time and solar illumination conditions could further elucidate trends in spectral magnitude shifts.

4.3. Future Surface Reflectance Validation Efforts

Calibration and validation of the EMIT surface reflectance product will be an ongoing process to ensure that the instrument is spectrally stable and accurate throughout the life of the mission. There are ongoing EMIT field campaigns

across the western United States that will provide additional insight into the surface reflectance product's performance in heterogeneous vegetated observing conditions. Spatiotemporally coincident observations between EMIT and other airborne (Airborne Visible/Infrared Imaging Spectrometer, AVIRIS) and spaceborne (EnMAP, DESIS, HiSUI) imaging spectrometers could provide an interesting comparison of surface reflectance products from different instruments. There may also be opportunities to exploit spatially coincident EMIT and historical AVIRIS imagery, particularly in the western United States

5. Conclusion

This work assessed the accuracy of surface reflectance products from the EMIT imaging spectrometer using three unique validation data sets: pseudoinvariant calibration sites, spectrometry conducted at selected field sites, and an automated radiometric calibration site. We have demonstrated that approximately 3% of surface reflectance error can be attributed to random atmospheric correction and instrument noise errors using pseudoinvariant calibration sites across northern Africa. We showed that EMIT surface reflectance at a typical arid land scene has a standard reflectance error of ±1.0% for coincident observations, rising to ±2.7% for data acquired on different dates and times of the day. We find that spectral magnitude shifts are often the core of this discrepancy, which is broadly consistent with BRDF effects due to changing solar position. An error budget that incorporated EMIT and ASD spectrometer uncertainties (e.g., BRDF, surface inhomogeneity, and calibration errors) encapsulated the variability between the two instruments in nearly all cases. Future surface reflectance algorithm improvements are planned, and long-term validation of the EMIT reflectance product will be an ongoing effort. Based on our systematic error analysis of the EMIT surface reflectance product, the vicarious calibration concept and novel atmospheric correction algorithms used for EMIT are highly successful and may pave the way for future orbital imaging spectrometer missions.

6. Code and Data Availability

The EMIT science data system code, including the code for generating Level 2 surface reflectance products can be found at `https://github.com/emit-sds/`. The open source code for optimal estimation atmospheric correction can be found online at `https://github.com/isofit/isofit`. USGS calibration site data are available as USGS data releases at:

- `https://doi.org/https://doi.org/10.5066/P96TLZOY`
- `https://doi.org/https://doi.org/10.5066/P9E2TSDF`
- `https://doi.org/https://doi.org/10.5066/P96XOJ6H`
- `https://doi.org/https://doi.org/10.5066/P90V4KUG`
- `https://doi.org/https://doi.org/10.5066/P95VM4OJ`

7. Acknowledgment

EMIT is supported by the National Aeronautics and Space Administration Earth Venture Instrument program, under the Earth Science Division of the Science Mission Directorate. Carlos Pérez García-Pando acknowledges support from the European Research Council (ERC) Consolidator Grant FRAGMENT (grant agreement No. 773051), and the AXA Chair on Sand and Dust Storms at the Barcelona Supercomputing Center funded by the AXA Research Fund. We thank Jeffrey Czapla-Myers and the University of Arizona team for their maintenance and operation of the Railroad Valley automated calibration facility. The research was carried out at the Jet Propulsion Laboratory, California Institute of Technology, under a contract with the National Aeronautics and Space Administration (80NM0018D0004). We acknowledge the support and assistance of NASA's International Space Station Program. The USGS authors' contribution was prepared as part of their official duties as U.S. Federal employees and constitutes a "work of the United States government," and is considered to be in the public domain and therefore domestic copyright does not apply. Any use of trade, firm, or product names is for descriptive purposes only and does not imply endorsement by the U.S. Government.

8. CRediT Author Statement

Red Willow Coleman: Writing - Original Draft, Methodology, Formal Analysis, Visualization, Validation, **David R. Thompson**: Methodology, Conceptualization, Writing - Original Draft, **Philip G. Brodrick**: Software, Data Curation, Writing - Review & Editing **Eyal Ben-Dor**: Investigation, **Evan Cox**: Investigation, **Carlos Pérez García-Pando**: Writing - Review & Editing, **Todd Hoefen**: Investigation, **Raymond Kokaly**: Investigation, **John M. Meyer**: Investigation, **Francisco Ochoa**: Investigation, **Gregory S. Okin**: Investigation, **Daniela Heller Pearlshtien**: Investigation, **Gregg Swayze**: Investigation, **Robert O. Green**: Supervision, Funding Acquisition

References

[1] R. O. Green, N. Mahowald, C. Ung, D. R. Thompson, L. Bator, M. Bennet, M. Bernas, N. Blackway, C. Bradley, J. Cha, et al., The earth surface mineral dust source investigation: An earth science imaging spectroscopy mission, in: 2020 IEEE aerospace conference, IEEE, 2020, pp. 1–15.

[2] T. Storch, H.-P. Honold, S. Chabrillat, M. Habermeyer, P. Tucker, M. Brell, A. Ohndorf, K. Wirth, M. Betz, M. Kuchler, et al., The enmap imaging spectroscopy mission towards operations, Remote Sensing of Environment 294 (2023) 113632.

[3] T. Matsunaga, A. Iwasaki, S. Tsuchida, K. Iwao, J. Tanii, O. Kashimura, R. Nakamura, H. Yamamoto, S. Kato, K. Obata, et al., Current status of hyperspectral imager suite (hisui) onboard international space station (iss), in: 2017 IEEE international geoscience and remote sensing symposium (IGARSS), IEEE, 2017, pp. 443–446.

[4] K. Alonso, M. Bachmann, K. Burch, E. Carmona, D. Cerra, R. De los Reyes, D. Dietrich, U. Heiden, A. Hölderlin, J. Ickes, et al., Data products, quality and validation of the dlr earth sensing imaging spectrometer (desis), Sensors 19 (20) (2019) 4471.

[5] J. Nieke, M. Rast, Towards the copernicus hyperspectral imaging mission for the environment (chime), in: Igarss 2018-2018 ieee international geoscience and remote sensing symposium, IEEE, 2018, pp. 157–159.

[6] K. Cawse-Nicholson, P. A. Townsend, D. Schimel, A. M. Assiri, P. L. Blake, M. F. Buongiorno, P. Campbell, N. Carmon, K. A. Casey, R. E. Correa-Pabón, et al., Nasa's surface biology and geology designated observable: A perspective on surface imaging algorithms, Remote Sensing of Environment 257 (2021) 112349.

[7] D. Heller Pearlshtien, E. Ben-Dor, Calval evaluation of desis products in amiaz plain and makhtesh ramon test sites, southern israel, The International Archives of the Photogrammetry, Remote Sensing and Spatial Information Sciences 46 (2022) 13–21.

[8] S. Cogliati, F. Sarti, L. Chiarantini, M. Cosi, R. Lorusso, E. Lopinto, F. Miglietta, L. Genesio, L. Guanter, A. Damm, et al., The prisma imaging spectroscopy mission: Overview and first performance analysis, Remote sensing of environment 262 (2021) 112499.

[9] D. S. Connelly, D. R. Thompson, N. M. Mahowald, L. Li, N. Carmon, G. S. Okin, R. O. Green, The emit mission information yield for mineral dust radiative forcing, Remote Sensing of Environment 258 (2021) 112380.

[10] L. Li, N. M. Mahowald, R. L. Miller, C. Pérez García-Pando, M. Klose, D. S. Hamilton, M. Gonçalves Ageitos, P. Ginoux, Y. Balkanski, R. O. Green, et al., Quantifying the range of the dust direct radiative effect due to source mineralogy uncertainty, Atmospheric chemistry and physics 21 (5) (2021) 3973–4005.

[11] D. R. Thompson, R. O. Green, C. Bradley, P. G. Brodrick, N. Mahowald, E. B. Dor, M. Bennett, M. Bernas, N. Carmon, K. D. Chadwick, R. N. Clark, R. W. Coleman, E. Cox, E. Diaz, M. L. Eastwood, R. Eckert, B. L. Ehlmann, P. Ginoux, M. G. Ageitos, K. Grant, L. Guanter, D. H. Pearlshtien, M. Helmlinger, H. Herzog, T. Hoefen, Y. Huang, A. Keebler, O. Kalashnikova, D. Keymeulen, R. Kokaly, M. Klose, L. Li, S. R. Lundeen, J. Meyer, E. Middleton, R. L. Miller, P. Mouroulis, B. Oaida, V. Obiso, F. Ochoa, W. Olson-Duvall, G. S. Okin, T. H. Painter, C. Pérez García-Pando, R. Pollock, V. Realmuto, L. Shaw, P. Sullivan, G. Swayze, E. Thingvold, A. K. Thorpe, S. Vannan, C. Villarreal, C. Ung, D. W. Wilson, S. Zandbergen, On-orbit calibration and performance of the emit imaging spectrometer, Remote Sensing of Environment 303 (2024) 113986. doi:https://doi.org/10.1016/j.rse.2023.113986.
URL https://www.sciencedirect.com/science/article/pii/S0034425723005382

[12] D. R. Thompson, V. Natraj, R. O. Green, M. C. Helmlinger, B.-C. Gao, M. L. Eastwood, Optimal estimation for imaging spectrometer atmospheric correction, Remote Sensing of Environment 216 (2018) 355–373. doi:https://doi.org/10.1016/j.rse.2018.07.003.

[13] H. Cosnefroy, M. Leroy, X. Briottet, Selection and characterization of saharan and arabian desert sites for the calibration of optical satellite sensors, Remote Sensing of Environment 58 (1) (1996) 101–114. doi:https://doi.org/10.1016/0034-4257(95)00211-1.

[14] K. Thome, Calibration/validation error budgets, uncertainties, traceability and their importance to imaging spectrometry, in: 2016 IEEE International Geoscience and Remote Sensing Symposium (IGARSS), IEEE, 2016, pp. 1912–1915.

[15] D. Helder, K. J. Thome, N. Mishra, G. Chander, X. Xiong, A. Angal, T. Choi, Absolute radiometric calibration of landsat using a pseudo invariant calibration site, IEEE Transactions on Geoscience and Remote Sensing 51 (3) (2013) 1360–1369.

[16] C. L. Bradley, E. Thingvold, L. B. Moore, J. M. Haag, N. A. Raouf, P. Mouroulis, R. O. Green, Optical design of the earth surface mineral dust source investigation (emit) imaging spectrometer, in: Imaging Spectrometry XXIV: Applications, Sensors, and Processing, Vol. 11504, SPIE, 2020, p. 1150402.

[17] C. D. Rodgers, Inverse methods for atmospheric sounding: theory and practice, Vol. 2, World scientific, 2000.

[18] P. G. Brodrick, D. R. Thompson, J. E. Fahlen, M. L. Eastwood, C. M. Sarture, S. R. Lundeen, W. Olson-Duvall, N. Carmon, R. O. Green, Generalized radiative transfer emulation for imaging spectroscopy reflectance retrievals, Remote Sensing of Environment 261 (2021) 112476.

[19] A. Berk, F. Hawes, Validation of modtran® 6 and its line-by-line algorithm, Journal of Quantitative Spectroscopy and Radiative Transfer 203 (2017) 542–556.

[20] D. R. Thompson, K. Babu, A. J. Braverman, M. L. Eastwood, R. O. Green, J. M. Hobbs, J. B. Jewell, B. Kindel, S. Massie, M. Mishra, et al., Optimal estimation of spectral surface reflectance in challenging atmospheres, Remote Sensing of Environment 232 (2019) 111258.

[21] D. R. Thompson, N. Bohn, P. G. Brodrick, N. Carmon, M. L. Eastwood, R. Eckert, C. G. Fichot, J. P. Harringmeyer, H. M. Nguyen, M. Simard, et al., Atmospheric lengthscales for global vswir imaging spectroscopy, Journal of Geophysical Research: Biogeosciences 127 (6) (2022) e2021JG006711.

[22] D. R. Thompson, K. Cawse-Nicholson, Z. Erickson, C. G. Fichot, C. Frankenberg, B.-C. Gao, M. M. Gierach, R. O. Green, D. Jensen, V. Natraj, et al., A unified approach to estimate land and water reflectances with uncertainties for coastal imaging spectroscopy, Remote Sensing of Environment 231 (2019) 111198.

[23] E. Greenberg, D. R. Thompson, D. Jensen, P. A. Townsend, N. Queally, A. Chlus, C. G. Fichot, J. P. Harringmeyer, M. Simard, An improved scheme for correcting remote spectral surface reflectance simultaneously for terrestrial brdf and water-surface sunglint in coastal environments, Journal of Geophysical Research: Biogeosciences 127 (3) (2022) e2021JG006712.

[24] J. P. Harringmeyer, N. Ghosh, M. W. Weiser, D. R. Thompson, M. Simard, S. E. Lohrenz, C. G. Fichot, A hyperspectral view of the nearshore mississippi river delta: Characterizing suspended particles in coastal wetlands using imaging spectroscopy, Remote Sensing of Environment 301 (2024) 113943.

[25] R. Eckert, S. Mauceri, D. R. Thompson, J. E. Fahlen, P. G. Brodrick, Spatially constrained atmosphere and surface retrieval for imaging spectroscopy, Remote Sensing of Environment 300 (2024) 113902.

[26] P. G. Brodrick, D. R. Thompson, R. W. Coleman, R. O. Green, et al., Surface reflectance and atmospheric modeling for the earth surface mineral dust source investigation (emit), Remote Sensing of Environment (2024 (in prep)).

[27] R. W. Johnson, An introduction to the bootstrap, Teaching statistics 23 (2) (2001) 49–54.

[28] C. Bacour, X. Briottet, F.-M. Bréon, F. Viallefont-Robinet, M. Bouvet, Revisiting pseudo invariant calibration sites (pics) over sand deserts for vicarious calibration of optical imagers at 20 km and 100 km scales, Remote Sensing 11 (10) (2019). doi:10.3390/rs11101166.

[29] P. Khakurel, L. Leigh, M. Kaewmanee, C. T. Pinto, Extended pseudo invariant calibration site-based trend-to-trend cross-calibration of optical satellite sensors, Remote Sensing 13 (8) (2021). doi:10.3390/rs13081545.

[30] M. Bouvet, K. Thome, B. Berthelot, A. Bialek, J. Czapla-Myers, N. P. Fox, P. Goryl, P. Henry, L. Ma, S. Marcq, A. Meygret, B. N. Wenny, E. R. Woolliams, Radcalnet: A radiometric calibration network for earth observing imagers operating in the visible to shortwave infrared spectral range, Remote Sensing 11 (20) (2019). doi:10.3390/rs11202401.

[31] J. M. Meyer, R. F. Kokaly, T. M. Hoefen, E. M. Cox, G. A. Swayze, Reflectance spectra collected august 17, 2022, at carson sink, nevada, with an asd fieldspec 4 hi-res ng spectrometer for calibration/validation of imaging spectrometer data, U.S. Geological Survey (2023). doi:https://doi.org/10.5066/P96TLZOY.

[32] J. M. Meyer, R. F. Kokaly, T. M. Hoefen, E. M. Cox, G. A. Swayze, Reflectance spectra collected august 16, 2022, at smith creek valley, nevada, with an asd fieldspec 4 hi-res ng spectrometer for calibration/validation of imaging spectrometer data, U.S. Geological Survey (2023). doi:https://doi.org/10.5066/P9E2TSDF.

[33] J. M. Meyer, R. F. Kokaly, T. M. Hoefen, E. M. Cox, G. A. Swayze, Reflectance spectra collected august 19, 2022, at edwards creek, nevada, with an asd fieldspec 4 hi-res ng spectrometer for calibration/validation of imaging spectrometer data, U.S. Geological Survey (2023). doi:https://doi.org/10.5066/P96XOJ6H.

[34] J. M. Meyer, R. F. Kokaly, T. M. Hoefen, E. M. Cox, G. A. Swayze, Reflectance spectra collected august 23, 2022, at long valley, nevada, with an asd fieldspec 4 hi-res ng spectrometer for calibration/validation of imaging spectrometer data, U.S. Geological Survey (2023). doi:https://doi.org/10.5066/P90V4KUG.

[35] J. M. Meyer, R. F. Kokaly, T. M. Hoefen, E. M. Cox, D. B. Ensign, Reflectance spectra collected april 17, 2023, at coyote lake, california, with an asd fieldspec 4 hi-res ng spectrometer for calibration/validation of imaging spectrometer data, U.S. Geological Survey (2023). doi:https://doi.org/10.5066/P95VM4OJ.

[36] G. T. Georgiev, J. J. Butler, Long-term comparison of spectralon BRDF measurements in the ultraviolet, in: W. L. Barnes, J. J. Butler (Eds.), Earth Observing Systems IX, Vol. 5542, International Society for Optics and Photonics, SPIE, 2004, pp. 323 – 333. doi:10.1117/12.559920.
URL https://doi.org/10.1117/12.559920

[37] D. Helder, K. Thome, D. Aaron, L. Leigh, J. Czapla-Myers, N. Leisso, S. Biggar, N. Anderson, Recent surface reflectance measurement campaigns with emphasis on best practices, si traceability and uncertainty estimation, Metrologia 49 (2) (2012) S21. doi:10.1088/0026-1394/49/2/S21.
URL https://dx.doi.org/10.1088/0026-1394/49/2/S21

[38] P. E. Dennison, D. A. Roberts, The effects of vegetation phenology on endmember selection and species mapping in southern california chaparral, Remote Sensing of Environment 87 (2) (2003) 295–309. doi:https://doi.org/10.1016/j.rse.2003.07.001.

[39] D. R. Thompson, K. Babu, A. J. Braverman, M. L. Eastwood, R. O. Green, J. M. Hobbs, J. B. Jewell, B. Kindel, S. Massie, M. Mishra, A. Mathur, V. Natraj, P. A. Townsend, F. C. Seidel, M. J. Turmon, Optimal estimation of spectral surface reflectance in challenging atmospheres, Remote Sensing of Environment 232 (2019) 111258. doi:https://doi.org/10.1016/j.rse.2019.111258.

[40] K. Gui, H. Che, Y. Wang, X. Xia, B. N. Holben, P. Goloub, E. Cuevas-Agulló, W. Yao, Y. Zheng, H. Zhao, L. Li, X. Zhang, A global-scale analysis of the misr level-3 aerosol optical depth (aod) product: Comparison with multi-platform aod data sources, Atmospheric Pollution Research 12 (12) (2021) 101238. doi:https://doi.org/10.1016/j.apr.2021.101238.

[41] P. G. Brodrick, D. R. Thompson, M. J. Garay, D. M. Giles, B. N. Holben, O. V. Kalashnikova, Simultaneous characterization of wildfire smoke and surface properties with imaging spectroscopy during the firex-aq field campaign, Journal of Geophysical Research: Atmospheres 127 (7) (2022) e2021JD034905, e2021JD034905 2021JD034905. doi:https://doi.org/10.1029/2021JD034905.

[42] J. Li, B. E. Carlson, Y. L. Yung, D. Lv, J. Hansen, J. E. Penner, H. Liao, V. Ramaswamy, R. A. Kahn, P. Zhang, O. Dubovik, A. Ding, A. A. Lacis, L. Zhang, Y. Dong, Scattering and absorbing aerosols in the climate system, Nat. Rev. Earth Environ. 3 (2022) 363–379. doi:10.1038/s43017-022-00296-7.

[43] R. N. Clark, G. A. Swayze, K. E. Livo, R. F. Kokaly, S. J. Sutley, J. B. Dalton, R. R. McDougal, C. A. Gent, Imaging spectroscopy: Earth and planetary remote sensing with the usgs tetracorder and expert systems, Journal of Geophysical Research: Planets 108 (E12) (2003). doi:https://doi.org/10.1029/2002JE001847.

[44] M. Berman, H. Kiiveri, R. Lagerstrom, A. Ernst, R. Dunne, J. Huntington, Ice: a statistical approach to identifying endmembers in hyper-

spectral images, IEEE Transactions on Geoscience and Remote Sensing 42 (10) (2004) 2085–2095. doi:10.1109/TGRS.2004.835299.

[45] R. N. Clark, T. L. Roush, Reflectance spectroscopy: Quantitative analysis techniques for remote sensing applications, Journal of Geophysical Research: Solid Earth 89 (B7) (1984) 6329–6340. doi:https://doi.org/10.1029/JB089iB07p06329.

[46] R. L. Powell, D. A. Roberts, P. E. Dennison, L. L. Hess, Sub-pixel mapping of urban land cover using multiple endmember spectral mixture analysis: Manaus, brazil, Remote Sensing of Environment 106 (2) (2007) 253–267. doi:https://doi.org/10.1016/j.rse.2006.09.005.

[47] K. N. Youngentob, D. A. Roberts, A. A. Held, P. E. Dennison, X. Jia, D. B. Lindenmayer, Mapping two eucalyptus subgenera using multiple endmember spectral mixture analysis and continuum-removed imaging spectrometry data, Remote Sensing of Environment 115 (5) (2011) 1115–1128. doi:https://doi.org/10.1016/j.rse.2010.12.012.

[48] C. Lin, K. Tsogt, C.-I. Chang, An empirical model-based method for signal restoration of swir in asd field spectroradiometry, Photogrammetric Engineering and Remote Sensing 78 (2012) 119–127. doi:10.14358/PERS.78.2.119.